Available online at www.sciencedirect.com
ScienceDirect
Chemical Physics Letters 439 (2007) 110–114
CHEMICAL PHYSICS LETTERS
www.elsevier.com/locate/cplett

Electronic structure mechanism of spin-polarized electron transport in a Ni–C_{60}–Ni system

Haiying He [a], Ravindra Pandey [a,*], Shashi P. Karna [b,*]

[a] Department of Physics and Multi-scale Technology Institute, Michigan Technological University, Houghton, MI 49931, United States
[b] US Army Research Laboratory, Weapons and Materials Research Directorate, ATTN: AMSRD-ARL-WM, Aberdeen Proving Ground, MD 21005-5069, United States

Received 2 November 2006; in final form 13 March 2007
Available online 23 March 2007

Abstract

The nature of chemical bonding and its effect on spin-polarized electron transport in Ni–C_{60}–Ni are studied using density functional theory in conjunction with the Landauer–Büttiker formalism. The binding site on the C_{60} cage surface appears to have a strong influence on the electron tunneling current between Ni leads. The tunnel current has a much higher magnitude when Ni is bonded to hole sites (H6, H5) than at bridge sites (B66, B56) of the fullerene cage. Furthermore, the magnitude of junction magnetoresistance is predicted to be significantly high for the molecular Ni–C_{60}–Ni system.

1. Introduction

In a recent experiment, Pasupathy et al. [1] reported the observation of C_{60}-mediated spin-dependent tunneling between ferromagnetic electrodes. Among other interesting features, the experiments [1,2] and theoretical predictions [3] demonstrated that C_{60} molecules strongly couple with metallic electrodes (e. g. Ni and Au), a key requirement for the Kondo effect. At the molecular scale, a goal of achieving a controlled assembly of such spintronic devices, however, requires a detailed and systematic understanding of the interfacial chemistry of the molecule and contact configurations and its role in the spin-polarized electron transport. This becomes even more important in the case of C_{60}, which offers a number of chemically different binding sites on the cage surface. For example, the B66 site is the bridge site over a C=C double bond, the B56 site is the bridge site over a C–C single bond, the H5 site is the hole site above the center of a pentagonal ring of C atoms, and the H6 site is the hole site above the center of a hexagonal ring of C atoms (see Fig. 1). In a strong coupling regime involving Ni–C_{60}–Ni, various possibilities of bonding exist between the Ni atoms of the lead and a C_{60} cage. In this letter, we examine the electronic structure mechanism of spin-polarized electron transport in Ni–C_{60}–Ni, focusing on the role of chemical bonding in electron transport. Our calculations reveal that the C_{60}-assisted tunnel current between Ni is facilitated by metal-induced gap states (MIGS) between the highest occupied (HO) and lowest unoccupied (LU) molecular orbitals (MOs), which in turn depend strongly on the C_{60} binding sites for Ni.

2. Calculations

The electronic transport calculations on a C_{60} molecule coupled to semi-infinite Ni electrodes (Fig. 2) are performed using the density functional theory (DFT) with the B3LYP functional form [4,5] in conjunction with the Landauer–Büttiker multi-channel formalism [6–8]. The core scattering region was simulated by the extended molecular complex (Ni_n–C_{60}–Ni_n) where atomic scale contacts were used for the molecule. The LanL2DZ basis sets were used for C and Ni. The symmetry-constrained

* Corresponding authors. Fax: +1 906 487 2933 (R. Pandey), +1 410 306 0723 (S.P. Karna).
E-mail addresses: pandey@mtu.edu (R. Pandey), skarna@arl.army.mil (S.P. Karna).

0009-2614/$ - see front matter © 2007 Elsevier B.V. All rights reserved.
doi:10.1016/j.cplett.2007.03.060

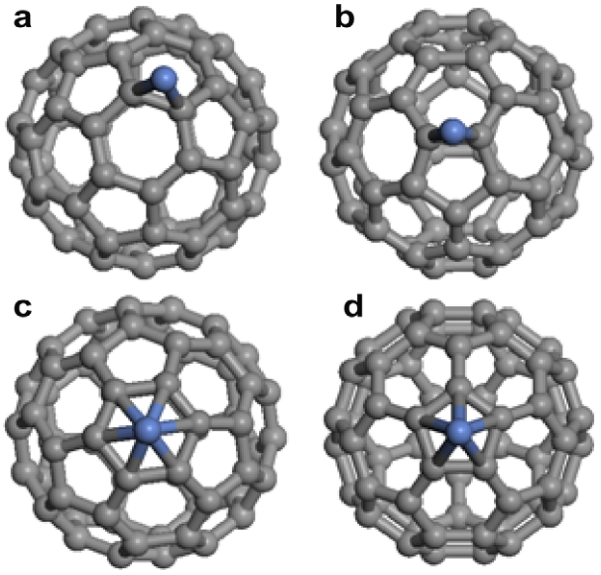

Fig. 1. Binding sites of Ni on C_{60}: (a) B66 – a bridge site over a C=C double bond, (b) B56 – a bridge site over a C–C single bond, (c) H6 – a hole site above the center of a hexagonal ring of C atoms and (d) H5 – a hole site above the center of a pentagonal ring of C atoms.

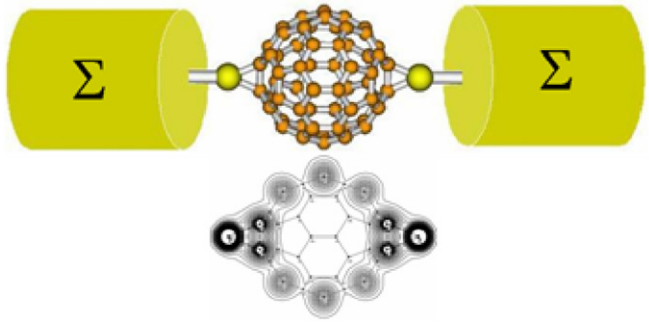

Fig. 2. A schematic illustration of a Ni–C_{60}–Ni molecular device. Top: The left/ right contact region is modeled by a Ni atom and the rest of the semi-infinite electrode is a Ni bulk reservoir, described by an effective self-energy Σ. Bottom: A slice of the charge density plots of the core scattering region is shown for the B66 binding site of C_{60}.

geometry optimization was performed using GAUSSIAN 03 [9] for the singlet spin-state representing the anti-parallel (AP) spin-alignment and triplet spin state representing the parallel (P) spin-alignment of the Ni atomic contacts in the system.

Since the bulk Ni metal is a ferromagnetic material having unbalanced spin-up (↑) and spin-down (↓) electrons near its Fermi level, the tunneling channels for spin-up (↑) and spin-down (↓) electrons were explicitly separated in transport calculations. The total current in such a device can be obtained by a summation of the contributions from both the spin-up ($I^{\uparrow}$) and the spin-down ($I^{\downarrow}$) electrons, and is given by

$$I^{\uparrow(\downarrow)} = \frac{e}{h}\int_{-\infty}^{\infty} \mathrm{d}E T^{\uparrow(\downarrow)}(E,V)[f(E-\mu_1) - f(E-\mu_2)]$$

where μ_1 and μ_2 are the electrochemical potentials in the two contacts under an external bias V, $f(E)$ is the Fermi-Dirac distribution function. $T(E, V)$ is the electron transmission function which can be calculated from a knowledge of the molecular energy levels and their coupling to the metallic contacts. Additional details of the calculations can be found elsewhere [10,11].

The Ni leads were represented by a set of atoms, and the bulk effect was implicitly included by a term of self-energy Σ. Several test calculations on Ni_n–C_{60}–Ni_n yielded consistent results showing that the convergence of the transport properties even with a single Ni atom representing the atomic contact was reasonably well. Likewise, a small effect on the transmission function with the increase in the number of contact atoms was reported for the Al–C_{60}–Al system [12].

3. Results and discussion

3.1. Ni–C_{60}–Ni bonding

The results predict that the bridge site over a C=C double bond (i.e. B66) to be the most stable site, which is followed by B56, H5 and H6 sites of the C_{60} molecule. This is consistent with the behavior of most transition metals towards C_{60} [13], where the C_{60} molecule acts as an η^2 ligand, forming two Ni–C bonds [14].

The singlet spin-state is always found to be lower in energy compared to the triplet spin-state. We note here that the Ni atoms have non-zero magnetic moment aligned in parallel to each other in the triplet spin-state. On the other hand, a strong hybridization of Ni-3d states with C-2p states leads to almost zero magnetic moment on Ni atoms in the singlet spin state of the system.

The binding energy of Ni–C_{60}–Ni with respect to the constituent atoms is positive (~6 eV) indicating the stability of the system. The bond length, R_{Ni-C}, shows dependence on the binding site; it increases with the increase in the Ni coordination number from two associated with the B66 and B56 sites to 6 associated with the H6 site. At the B66 site, the bridge C=C bond is actually broken, and the bond length R_{C-C} increases from 1.40 to 1.49 Å which is in the order of the C–C single bond length. The Natural Bond Orbital (NBO) analysis suggests the formation of Ni–C bond with a bond order of 0.7. At the H6 site, on the other hand, the d – π orbital interaction only leads to slightly change in bond length in the hexagonal ring.

The Mulliken population analysis shows that C_{60} acts as an electron acceptor. In the ground state of the isolated C_{60} molecule, the electronic configuration has a threefold degenerate LUMO, t_u and a fivefold degenerate HOMO, h_u. The degeneracy in C_{60}–LUMO is lifted by the interaction between Ni and C atoms resulting into a partial occupation of C_{60}–LUMO in Ni–C_{60}–Ni. In addition to the fact that the charge transfer from Ni to C is slightly larger for the H6 site relative to the B66 site, it may also be worthy to point out that the charge distribution pattern is quite different for the two binding sites. In the case of the bridge

site, the nearest-neighbor (nn) C atoms have additional charge than what is transferred from a bonded Ni atom. The additional charge was provided by four second-neighbor (2n) C atoms. Since the device is neutrally charged, the rest of the C atoms of the fullerene molecule were slightly negatively charged. For hole binding sites, six 2n C atoms accept the charge transfer from the bonded Ni atom, while the six nn-C atoms remain slightly positively charged. The rest of the C atoms of the fullerene molecule remain almost neutral. The binding of Ni contact atom(s) at B66 and H6 sites therefore exhibits different interfacial features in Ni–C_{60}–Ni. At the bridge site, the charge transfer occurs mostly at the interface atoms where bonding between the Ni and the fullerene takes place, whereas 2n C atoms are mainly involved in the charge transfer process at the H6 site. This unique feature at the H6 site reflects a long-range interaction, which is a reminiscence of the long-range bound state in a Ni–benzene complex predicted by both electric deflection experiments and CASSCF + MRCI calculations [15].

3.2. Transmission function (T)

The calculated transmission functions are shown in Fig. 3a,b for the P and the AP spin orientations of the molecular system, respectively. The transmission function, in general, reflects the intrinsic transmission characteristics of the fullerene molecule despite the differences in the binding characteristics at the Ni–C_{60} interface. The HOMO–LUMO gap of the isolated C_{60} molecule reflects itself in a vanishing transmission gap in the near Fermi region [12]. Electronic transport calculations were performed for all binding sites. Here, we only focus on the B66 and the H6 binding sites in the following discussion since they represent the two dominant bonding features for electron transport.

Analysis of the scattering states near the Fermi energy reveals their character to be associated with HOMO or LUMO of the system. A broad peak appears in the HOMO–LUMO gap region for the B66 site which becomes more pronounced for the H6 site in the case of the parallel orientation of the spin states of the atomic Ni contacts. Such a peak is usually identified as the metal-induced gap state (MIGS) [16] whose origin is attributed to the interaction between the molecule and the metallic electrodes. In order to explore the character of MIGS, we relate the calculated Kohn–Sham orbitals for the extended molecule to the calculated transmission function of the device in Fig. 3. More specifically shown in Fig. 3 are the molecular spectra of the device consisting of the pure molecule, the molecule–metal hybrid system, and the pure metal. Even though the carbon molecular orbitals have sharp and high peaks in transmission and will be mostly responsible for the resonance tunneling, the hybrid orbitals play an important role in the low-bias regime.

Analysis of molecular orbitals (Fig. 4) reveals that the MIGS arises due to hybridization of one of the C_{60}'s LUMO orbitals with Ni's 3d orbital, $3d_{xy}$ and $3d_{x_2-y_2}$ for the B66 and H6 cases, respectively. In the case of H6, the hybrid LUMO is more extended leading to higher transmission for electrons tunneling through this eigen channel. A higher density of the hybrid states near E_f, hence larger number of tunneling channels, also appear to cause higher transmission for the H6 site relative to the B66 site in Ni–C_{60}–Ni.

3.3. Tunnel current (I)

The calculated tunneling current shown in Fig. 5 is significantly higher in the P spin configuration than that in the AP spin configuration for both the bridge and the hole binding sites, as we would expect from the transmission

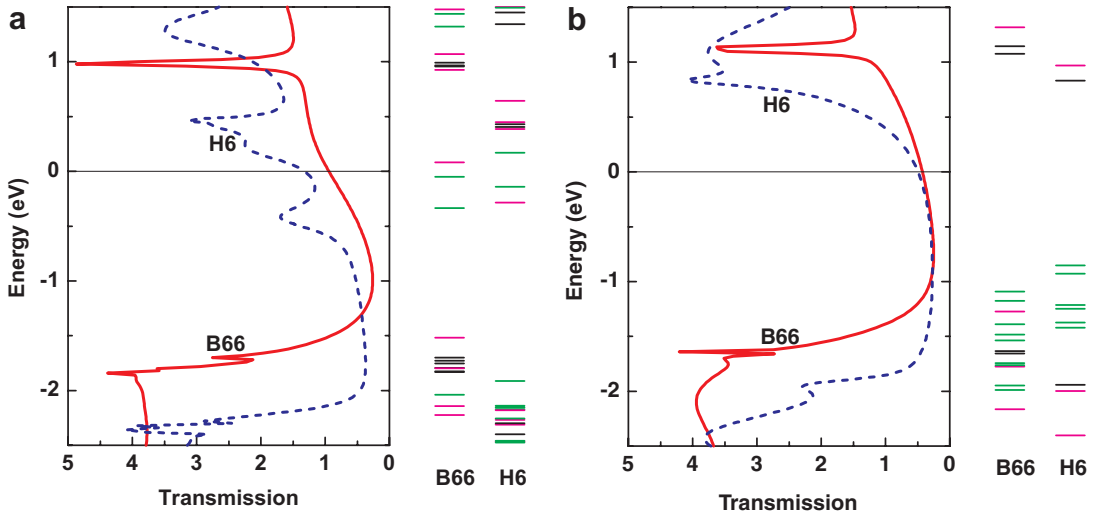

Fig. 3. Transmission functions for: (a) parallel (P) and (b) anti-parallel (AP) spin orientations of Ni leads in Ni–C_{60}–Ni. The Kohn–Sham orbitals are also given; pure C_{60} orbitals are in black, hybrid states are in magenta, and pure Ni orbitals are in green. The B66 and H6 are binding sites, and zero of the energy is aligned to the Fermi energy. (For interpretation of the references in colour in this figure legend, the reader is referred to the web version of this article.)

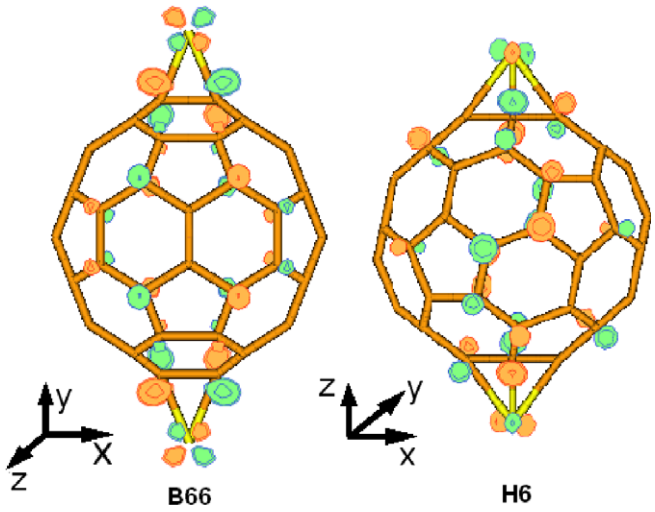

Fig. 4. Molecular orbitals for α-HOMOs of Ni–C_{60}–Ni in which Ni is bonded at B66 (left) and H6 (right) sites in the parallel (P) case. One of C_{60}'s LUMOs takes part in the hybridization with Ni $3d_{xy}$ and $3d_{x2-y2}$ to generate the metal induced gap states in Ni–C_{60}–Ni. The orientation of Cartesian coordinates is also given here.

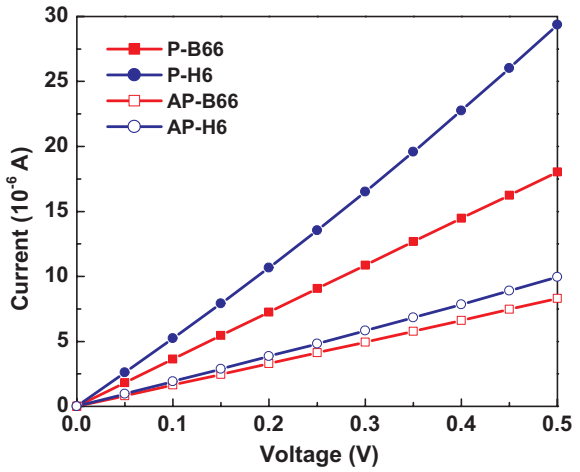

Fig. 5. Current–voltage curves for parallel (P) and anti-parallel (AP) spin orientations of Ni leads in Ni–C_{60}–Ni. The B66 and H6 are binding sites of C_{60}.

results. In addition, the tunnel current associated with the H6 site is higher than that associated with the B66 site in the device.

In the low bias region (<0.5 V), a linear response is observed for the P case, showing an Ohmic behavior. Such metal-like behavior has also been noted for Al–C_{60}–Al [17] and Au–C_{60}–Au junctions [18] in the low-bias regime. However, a closer look at the differential conductance suggests a slightly different trend in the variation of conductance with respect to the external bias voltage. The conductance for the B66 interface is almost constant, showing a metal-like behavior, whereas the conductance for H6 has a relatively large fluctuation in going from zero to higher biases, indicating a tunneling behavior of the electron transport. This difference is a direct reflection of the sharper peak in the transmission function in the vicinity region of E_f for H6 relative to B66 as shown in Fig. 3.

In the AP case, a linear response in I–V curve in the low bias regime is well preserved. However, the differential conductance dI/dV decreases significantly compared to the P case, due to the absence of the MIGS. The equilibrium conductance values for B66 (H6) are 0.47 (0.67) for the P case and 0.21 (0.25) for the AP case, in terms of $G_0 = 2e^2/h$. These values are in reasonably good agreement with those reported for Au–C_{60}–Au junctions ($\sim G_0$) [18], since Ni has a slightly larger work function (~5.5 eV) than Au (~5.3 eV). We note that the order of the predicted current in the AP case is similar to what was previously calculated for Au–C_{60}–Au [18], and was measured for the electromechanic amplifier [19].

The calculated values of junction magnetoresistance (JMR) (i.e. $(G_P - G_{AP})/G_{AP}$) are positive, as usually found in magnetic tunnel junctions. The magnitude of JMR in Ni–C_{60}–Ni is significantly large among the molecules so far studied; the configuration with Ni binding at H6 site of the fullerene molecule has the JMR of about 200%.

4. Summary

We have studied the electronic structure mechanism in the strongly coupled regime for C_{60}-mediated spin-dependent electron transport between Ni leads with the use of density functional theory and the Landauer–Büttiker formalism. The calculated results clearly show that the magnitude of the tunnel current strongly depends on the details of the molecule–electrode interface at the atomic scale as well as the spin alignment of the two ferromagnetic electrodes. Chemical bonding in the Ni–C_{60}–Ni system, where a participating metal atom could interact with a larger number of C atoms on the C_{60} surface, offers a larger value of tunneling current. Such a site is realized for the H6 position on the C_{60} surface. The results also suggest a large magnitude of JMR in the case of Ni–C_{60}–Ni system, in agreement with the experiment [1]. Metal-induced gap states, which lead to higher tunneling current in the parallel spin alignment, are also closely related to the nature of the chemical bonding between the metal and C_{60} molecule. Although the importance of the molecule-electrode interface is well acknowledged in studies of the single molecule conductance, the accurate control and precise characterization of interfacial features are still under a very immature stage in experiments [2]. From this aspect, theoretical studies may provide not only an indispensable tool to analyze and interpret the experimental results, but also valuable guidelines in docking molecules on electrodes.

Acknowledgements

The work at Michigan Technological University was performed under support by the DARPA through contract number ARL-DAAD17-03-C-0115. The work at Army Research Laboratory (ARL) was supported by the DARPA

MoleApps program and ARL-Director's Research Initiative-FY05-WMR01. Helpful discussions with S. Gowtham, K.C. Lau and R. Pati are acknowledged.

References

[1] A.N. Pasupathy, R.C. Bialczak, J. Martinek, J.E. Grose, L.A.K. Donev, P.L. McEuen, D.C. Ralph, Science 306 (2004) 86.
[2] L.H. Yu, D. Natelson, Nanoletter 4 (2004) 79.
[3] Y. Utsumi, J. Martinek, G. Schön, H. Imamura, S. Maekawa, Phys. Rev. B 71 (2005) 245116.
[4] A.D. Becke, J. Chem. Phys. 98 (1993) 5648.
[5] C. Lee, W. Yang, R.G. Parr, Phys. Rev. B 37 (1998) 785.
[6] R. Landauer, J. Phys.: Condens. Matter 1 (1989) 8099.
[7] M. Büttiker, Phys. Rev. Lett. 57 (1986) 1761.
[8] S. Datta, Electronic Transport Properties in Mesoscopic Systems, Cambridge University Press, Cambridge, 1995.
[9] M.J. Frisch et al., GAUSSIAN 03, Gaussian, Inc., Pittsburgh, PA, 2003.
[10] W. Tian, S. Datta, S. Hong, R. Reifenberger, J.I. Henderson, C.P. Kubiak, J. Chem. Phys. 109 (1998) 2874.
[11] H. He, R. Pandey, R. Pati, S.P. Karna, Phys. Rev. B 73 (2006) 195311.
[12] J.J. Palacios, A.J. Pérez-Jiménez, E. Louis, J.A. Vergés, Phys. Rev. B 64 (2001) 115411.
[13] P. Mathur, I.J. Mavunkal, S.B. Umbarkar, J. Cluster Sci. 9 (1998) 393.
[14] M.M.G. Alemany, O. Die'guez, C. Rey, L.J. Gallego, J. Chem. Phys. 114 (2001) 9371.
[15] F. Rabilloud et al., J. Phys. Chem. A 107 (2003) 11347.
[16] S. Dag, O. Gülseren, S. Ciraci, T. Yildirim, Appl. Phys. Lett. 83 (2003) 3180.
[17] J. Taylor, H. Guo, J. Wang, Phys. Rev. B 63 (2001) 121104(R).
[18] N. Sergueev, D. Roubtsov, H. Guo, cond-mat/0309614.
[19] J.K. Gimzewski, C. Joachim, Science 283 (1999) 1683.